Surface & Coatings Technology 446 (2022) 128784

Contents lists available at ScienceDirect

Surface & Coatings Technology

journal homepage: www.elsevier.com/locate/surfcoat

Microstructure and mechanical properties of SiC particle reinforced Zr-based metallic glass surface composite layers produced by laser alloying

Yongfeng Qian [a], Di Zhang [a], Jing Hong [a], Lin Zhang [b], Minqiang Jiang [c,d], Hu Huang [a,*], Jiwang Yan [b]

[a] Key Laboratory of CNC Equipment Reliability, Ministry of Education, School of Mechanical and Aerospace Engineering, Electron Microscopy Center, Jilin University, Changchun, Jilin 130022, China
[b] Department of Mechanical Engineering, Faculty of Science and Technology, Keio University, Yokohama 223-8522, Japan
[c] State Key Laboratory of Nonlinear Mechanics, Institute of Mechanics, Chinese Academy of Sciences, Beijing 100190, China
[d] School of Engineering Science, University of Chinese Academy of Sciences, Beijing 100049, China

ARTICLE INFO

Keywords:
Metallic glass
SiC particle
Laser surface alloying
Ceramic phase
Hardness

ABSTRACT

Metallic glasses (MGs) are a promising candidate for advanced structural applications due to their superior mechanical properties. Improving their surface mechanical properties would be of great importance for promoting their structural and functional applications. In this study, SiC particles were used as the reinforcement to improve the mechanical properties of Zr-based MG via laser surface alloying. The influences of the average laser power and overlap ratio between neighboring laser processing lines on the microstructure and mechanical properties of the laser-alloyed surface layer were investigated. The experimental results indicated that ZrC and SiC phases were successfully introduced into the MG matrix by laser surface alloying, and the content of these two hard ceramic phases was dependent on the laser processing parameters. The formed laser-alloyed surface layers exhibited a significant improvement in overall hardness compared with the as-cast specimen. At a relatively high overlap ratio of 70%, the average hardness of the MG matrix within the laser-alloyed surface layer reached 28.91 GPa, which was three times higher than that of the as-cast specimen (6.46 GPa). Furthermore, the microstructural characteristics and mechanical properties of the cross-sections of the laser-alloyed samples were characterized. The thickness of the laser-alloyed surface layer reached several tens of microns, and the SiC particles were uniformly dispersed in the whole laser-alloyed surface layer. This study confirms the feasibility for improving the mechanical properties of MGs by laser surface alloying, which is expected to broaden the application of MGs as structural and functional components under harsh severe conditions.

1. Introduction

Unlike conventional crystalline materials with long-range translational symmetry, metallic glasses (MGs) inherit disordered atomic arrangements from the isotropic liquid state [1–3]. With the absence of crystalline defects that act as deformation carriers like dislocations and stacking faults, MGs exhibit more impressive mechanical properties compared with their crystalline counterparts [4–6], such as ultra-high strength and excellent anti-wear characteristics [7–9]. These superior properties enable a wide range of applications of MGs as structural materials [10,11], for instance, as components for defense weapons and sport products [11–13]. For practical engineering applications of MGs as structural materials, their surfaces will inevitably be exposed to harsh industrial working conditions for long periods of time. It has been well-documented that failure of structural materials usually originates from surface wear and damage [14,15]. Besides this, it is also widely recognized that the wear resistance of materials is dominated by their surface hardness [16–18]. Therefore, to improve the service reliability and prolong the service life of MGs, it is urgently required to improve their surface hardness. Besides the requirement to improve surface hardness, another pressing issue that needs to be addressed in most MG systems is their intrinsic brittleness at room temperature [19–21]. The negligible macroscopic plastic deformation capacity of MGs is primarily due to the rapid propagation of highly localized individual shear bands under loading, which is associated with the catastrophic failure of MGs. This seriously impedes their structural applications as advanced materials

* Corresponding author.
E-mail address: huanghu@jlu.edu.cn (H. Huang).

https://doi.org/10.1016/j.surfcoat.2022.128784
Received 18 July 2022; Received in revised form 4 August 2022; Accepted 10 August 2022
Available online 17 August 2022

[22–24]. Therefore, tailoring the mechanical properties of MGs to simultaneously improve surface hardness and plasticity is of great significance in both practical engineering application and laboratory fundamental research.

An effective approach for solving the above-mentioned problems is to introduce reinforcement phases into the MG matrix to form MG surface composites [25,26]. The micro/nano-scale secondary phases in MG composites can act as obstacles to impede the unmitigated propagation of shear bands initiated in the glass matrix [26,27], thus increasing the resistance to plastic deformation, which plays a crucial role in hardening the MG surface. On the other hand, the micro/nano-scale heterogeneity within the MG composites provides potential nucleation sites for the formation of multiple shear bands [28,29], and these shear bands can disperse the applied stress more homogeneously, which helps to improve the overall plasticity of MGs [5,30].

To synthesize MG composites, a large number of processing technologies have been successively explored and developed over the past decades [31,32]. For example, via arc melting using high-purity metal powders, Zhang et al. [23] prepared large-sized Ti-based MG composites, which exhibited a high strength and a simultaneous large plasticity. By spark plasma sintering, tungsten particle reinforced Zr-based MG composites were fabricated, which showed potential applications as armor-piercing materials [5]. In addition to the above-mentioned methods, the introduction of secondary phase into the MG matrix through the in-situ reaction between MGs and other elements under direct irradiation of high-energy laser beam has also attracted extensive attention due to its high efficiency and environmental friendliness [19,33]. For instance, by laser irradiation in a flowing nitrogen environment, surface composite layers containing ZrN phase with thicknesses of tens of micrometers could be prepared on a typical Zr-based MG substrate through the reaction between Zr and N elements, which changed the plastic deformation behaviors and significantly improved the surface hardness compared with the as-cast sample [33]. However, this method is highly dependent on the affinity between the elements in the MG matrix and the externally added elements, i.e., it lacks universal applicability. In comparison with this method, laser surface alloying technology may be more suitable for most kinds of MG systems to prepare surface composite layers due to its wide selection of materials [34]. This technology is a complex physical and chemical metallurgical process based on the principle of non-contact heating of the substrate surface with pre-coated powder using high-energy laser, followed by rapid solidification of the molten materials to produce an in-situ formed alloyed layer on the bulk substrate [35]. It is worth mentioning that in addition to good versatility, laser surface alloying technology has characteristics such as the minimal thermal effect and ultra-fast cooling rate [36], which offer the possibility of maintaining the properties of the bulk substrate.

The overall mechanical properties of the surface composite layer are strongly dependent on the selection of the reinforcement phases. As a typical ceramic-based hard particle, SiC has been extensively used to strengthen various materials due to its excellent combination of high strength and hardness, superior wear resistance and low cost [37–39]. However, until now, the use of laser surface alloying technology to fabricate MG surface composites containing SiC has been rarely investigated. In the present study, aiming at obtaining MG surface composites with good mechanical properties, a Zr-based MG was chosen as the base material and reinforced by SiC particles via laser surface alloying. The morphology, chemical compositions, surface hardness and cross-sectional characteristics of the surface composite layers obtained under different laser processing parameters were comparably investigated to understand the structure-property relationship. The experimental results showed that the overall hardness of the surface composite layers was significantly higher than that of the as-cast MG specimen, and accordingly, the underlying hardening mechanism was discussed. It is expected that the fabricated surface composite layers with enhanced mechanical properties can improve the service life of MGs as structural components under harsh severe conditions.

2. Experimental procedures

2.1. Specimen preparation and laser surface alloying process

In the experiments, the as-cast Vitreloy 1 MG ($Zr_{41.2}Ti_{13.8}Cu_{12.5}Ni_{10}Be_{22.5}$, in at. %) with dimensions of 20 mm × 20 mm × 2 mm was employed as the base material, with consideration of its excellent glass forming ability [40,41] and commercial availability. To remove possible surface oxides and achieve uniform spreading of SiC powder, the MG specimen was ground with a series of grit SiC papers (P400, P800, P1200, P2000, P3000) and subsequently polished with 0.5 μm diamond abrasive paste to obtain a mirror-like appearance with a surface roughness of ~4 nm. Commercially available SiC powder (99% purity) was used as reinforcement for the fabrication of surface composite layers. Figs. 1(a) and (b) present the morphology and particle size distribution of the SiC powder, respectively. The SiC particles exhibit an irregular polyhedral shape with an average size of 8.54 μm. The X-ray diffractogram in Fig. 1(c) reveals that the SiC powder is only composed of single SiC phase, confirming the absence of other impurities in the SiC powder.

The preparation route for the pre-coated powder layer is illustrated in Fig. 2(a). First, the SiC powder and deionized water were mixed in a mass ratio of 1:19. Next, the mixture was stirred thoroughly to obtain a homogeneous SiC suspension. Finally, the SiC suspension was injected into a container with a MG specimen placed at the bottom, followed by air drying for a long time to obtain a solidified powder layer. The thickness of the pre-coated powder layer could be easily controlled by adjusting the volume of the suspension injected into the container, and it was chosen to be 60 μm in the present study according to the results of some preliminary experiments.

The laser surface alloying experiments were performed by using a nanosecond pulsed fiber laser (SP-050P-A-EP-Z-F-Y, SPI Lasers, UK), which produced a Gaussian laser beam with central wavelength of 1064 nm, pulse duration of 7 ns, repetition rate of 800 kHz and spot size of about 43 μm. Fig. 2(b) presents the schematic representation of the laser processing system and the scanning strategy (i.e., zig-zag pattern) used during the experiments. The laser source was directed through a pair of mirrors and then focused by the F-theta lens onto the MG substrate pre-coated with SiC powder at normal incidence. Argon (99.999% purity) was used as the shielding gas during the experiments to minimize oxidation. To investigate the influence of average laser power and overlap ratio between neighboring laser processing lines on the microstructure and mechanical properties of the surface composite layer, three tested cases corresponding to different processing parameters were selected according to some pre-experiments. The detailed processing parameters are listed in Table 1.

2.2. Characterization of microstructure and mechanical properties

The surface and cross-sectional morphological characteristics of the fabricated surface composite layers were characterized by using a scanning electron microscope (SEM, JSM-IT500A, JEOL). The phase composition and elemental distribution of the fabricated surface composite layers were identified by a combination of energy dispersive X-ray spectrometer (EDS, EX-74600U4L2Q, JEOL), X-ray diffractometer (XRD, D8 Advance, Bruker) and Raman spectrometer (Alpha300 R, WITec). A nanoindentation instrument (DUH-211S, Shimadzu) equipped with a Berkovich-type indenter was employed to measure the surface and cross-sectional hardness of the fabricated surface composite layers in the load control mode. A maximum indentation force of 200 mN with a loading speed of 10 mN/s was applied. For statistical analysis, 30 nanoindentation measurements were performed for each case, and the corresponding average value with standard deviation was recorded. After nanoindentation measurement, the morphology of the residual indent

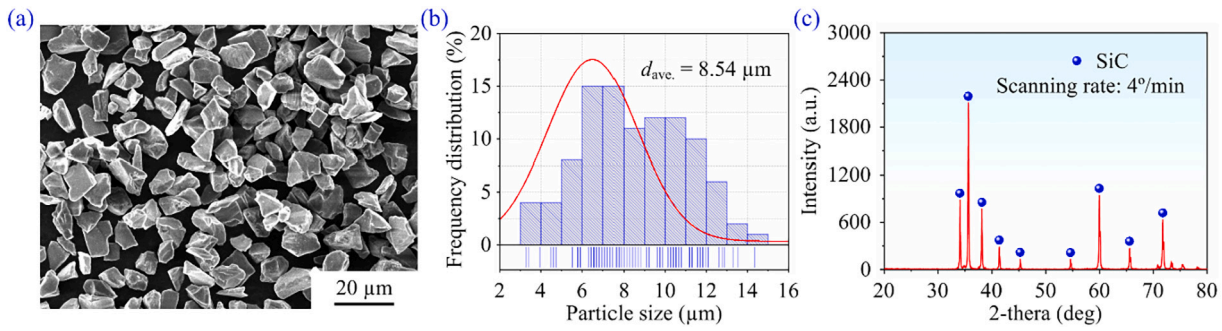

Fig. 1. (a) Morphology, (b) statistical particle size and (c) X-ray diffractogram of the SiC powder.

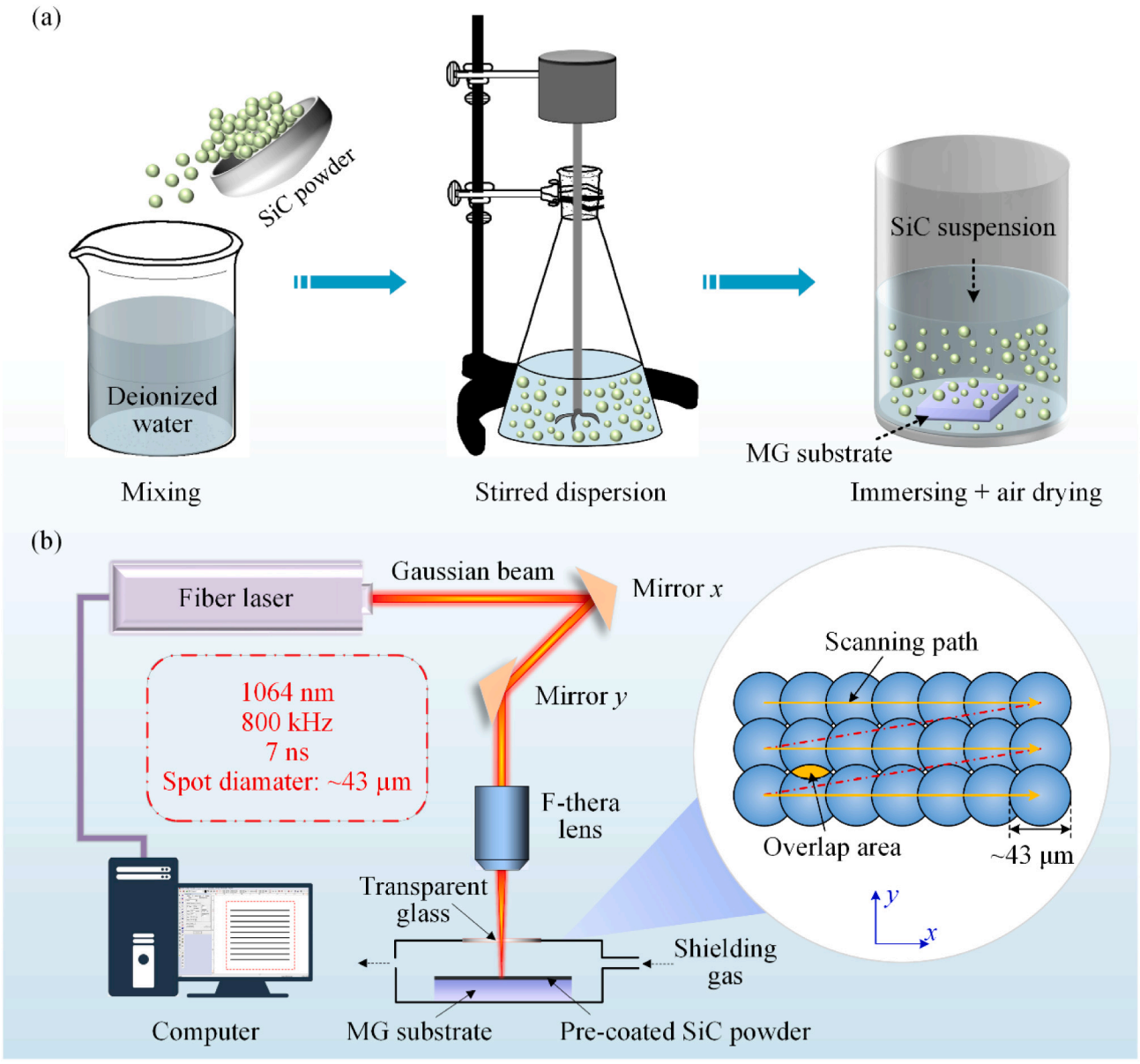

Fig. 2. (a) The preparation route for the pre-coated powder layer. (b) Schematic representation of the laser processing system and the scanning strategy used during the experiments.

Table 1
Detailed processing parameters for three selected cases.

	Average laser power (W)	Overlap ratio (%)	Scanning speed (mm/s)
A1	6.45	30	5
B1	10.30	30	5
C1	6.45	70	5

was observed by SEM to understand the underlying deformation behavior.

3. Results and discussion

Figs. 3(a)-(c) presents the SEM micrographs of the laser-alloyed surface layers corresponding to the three tested cases. A large number of micro-pores are observed for case A1, as indicated in Fig. 3(a). Being similar to the selective laser melting process, the formation of micro-pores during the laser surface alloying process is mainly due to the incomplete re-melting of some localized areas [42] and the unstable melt flow under the influence of driving forces such as Marangoni force and recoil pressure [43]. When increasing the average laser power (case B1) or overlap ratio (case C1), both the number and size of micro-pores decrease, as evidenced by the SEM micrographs shown in Figs. 3(b) and (c) as well as the statistical results of porosity for the three tested cases displayed in Fig. 3(d). This is due to that during the line-by-line laser scanning process, when a higher average laser power or a higher overlap ratio is employed, a more adequate melting of the target processing area is expected since more input energy will be consumed in melting the SiC particles and re-melting the micro-pores formed in the preceding line scanning process, resulting in a relatively low porosity. Moreover, it is worth noting that the high input energy and the resultant high temperature gradient will induce stronger thermal stress, which will promote the formation of micro-cracks [44,45], as indicated in Figs. 3(b) and (c).

As the laser-alloyed surface layers shown in Figs. 3(a)-(c) are quite rough and accompanied by undesirable micro-pores, they were mechanically polished prior to the subsequent characterization of chemical composition and mechanical properties. Figs. 4(a)-(c) present the SEM micrographs of these surface layers after polishing, where obvious micro-pores shown in Figs. 3(a)-(c) are not observed, suggesting that the subsurface layer of the laser-alloyed sample may be more dense than its top surface layer. Furthermore, the polished surfaces present two well-defined regions with remarkable difference in contrast: dark grey and light grey. In particular, in terms of geometric profile, the dark grey regions are very similar to the SiC particles shown in Fig. 1(a). Considering the high melting point of the SiC particles, it is inferred that these dark grey regions represent SiC particles that have not been completely decomposed during the laser surface alloying process [46]. Corresponding to the SEM micrographs displayed in Figs. 4(a)-(c), the statistical results of SiC particle size are shown in Figs. 4(d)-(f). For all three cases, the average size of the SiC particles within the laser-alloyed surface layers is significantly smaller than that of original SiC powder (8.54 μm), which confirms that the SiC particles might be partially decomposed during the laser surface alloying process. In addition, it is worth noting that the average size of the SiC particles for case B1 and case C1 is smaller than that for case A1, which could be due to that increasing the laser input energy will promote the decomposition of SiC particles [46].

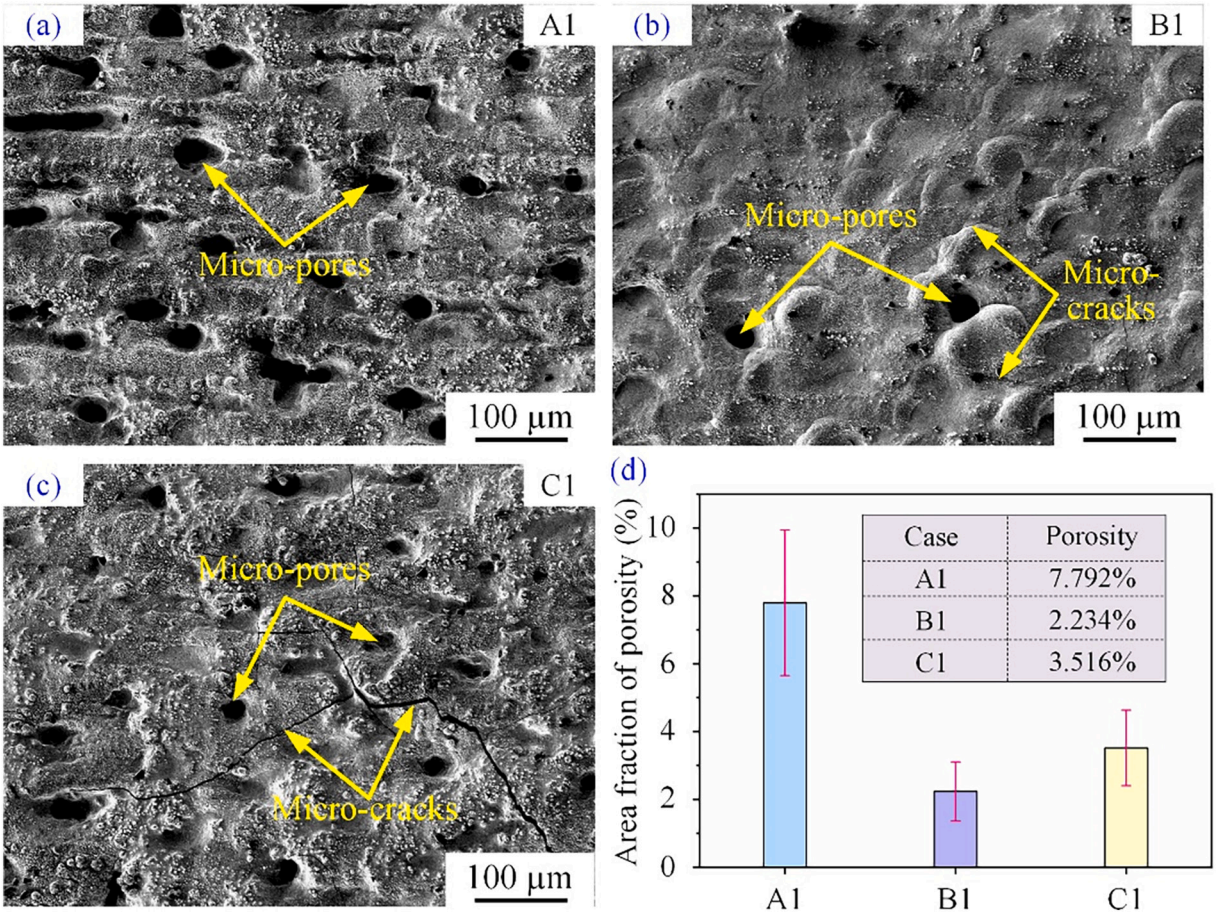

Fig. 3. SEM micrographs of the laser-alloyed surface layers corresponding to the three tested cases: (a) case A1, (b) case B1, and (c) case C1. (d) The statistical results of porosity for the three tested cases.

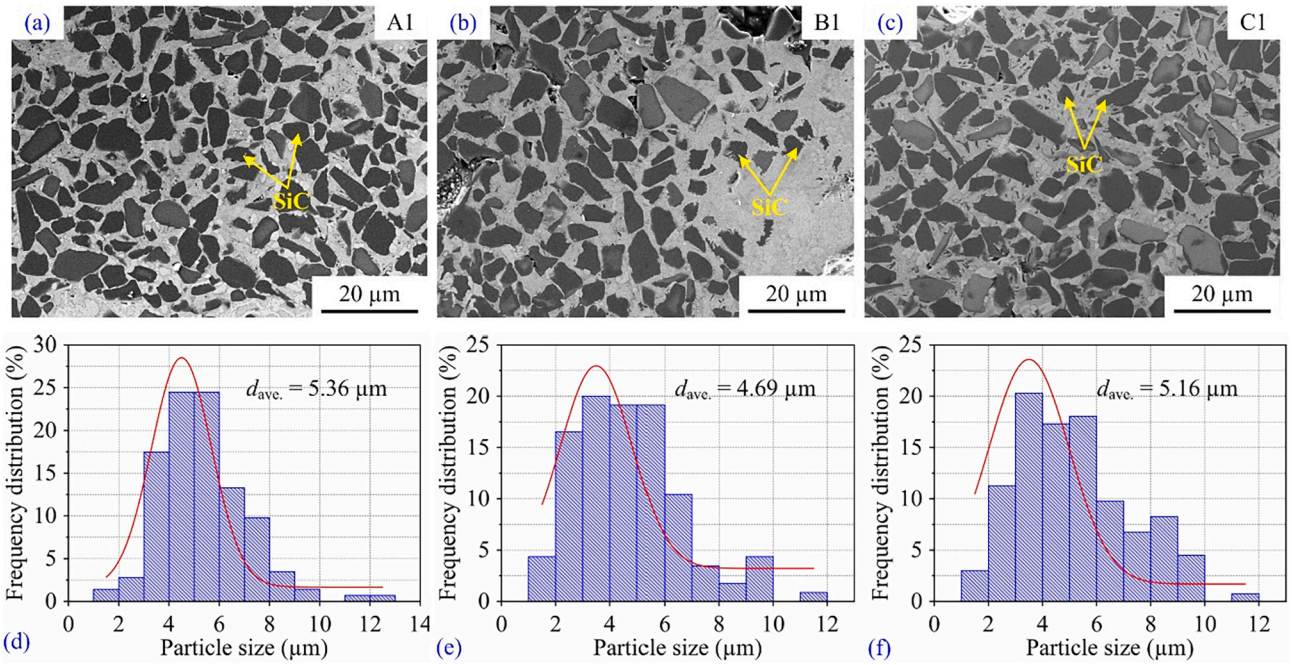

Fig. 4. SEM micrographs of the laser-alloyed surface layers after polishing, corresponding to the three tested cases: (a) case A1, (b) case B1, and (c) case C1. (d)-(f) The size distribution of SiC particles shown in Figs. 4(a)-(c).

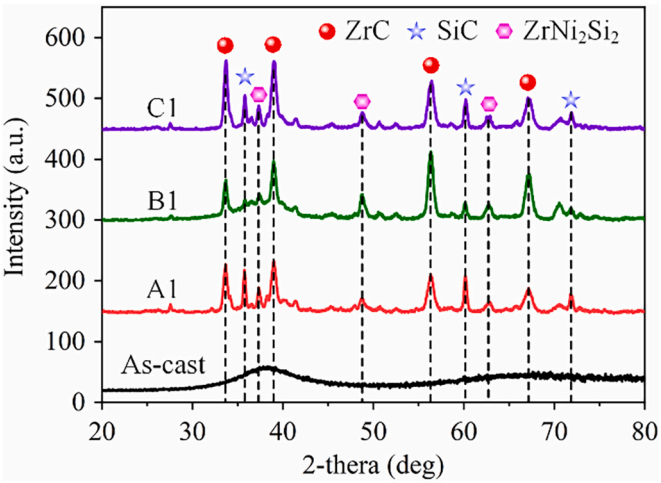

Fig. 5. XRD patterns of the laser-alloyed surface layers after polishing as well as the as-cast specimen.

To investigate the chemical composition evolution induced by laser surface alloying, the phases of the laser-alloyed surface layers after polishing were characterized by XRD and compared with the as-cast specimen. Fig. 5 presents the corresponding results. Being clearly distinguished from the broad diffraction hump without any trace of diffraction peaks exhibited on the XRD pattern of the as-cast specimen, some sharp crystalline peaks overlapping to the amorphous hump are observed for the three tested cases, indicating the existence of both crystalline and amorphous phases in the laser-alloyed surface layers. Meanwhile, for the three tested cases, the diffraction peaks located at the identical angular position suggest similar chemical compositions, and the corresponding dominant diffraction peaks can be well-indexed to the ZrC and SiC phases. Here, the SiC phase arises from incompletely decomposed SiC particles, and the ZrC phase may be formed by the in-situ reaction between the Zr atoms root in the MG matrix and the C atoms resulting from the decomposition of the SiC particle. In addition, the evident changes from case A1 to case B1 or Case C1 are that the intensity of ZrC phase is increased but the intensity of SiC phase is decreased, which indicates that the content of these crystalline phases is strongly dependent on the laser processing parameters.

The above XRD analysis results indicate that both ZrC and SiC phases have been introduced into the laser-alloyed surface layers after laser surface alloying. To further reveal the element composition of the dark and light grey regions shown in Figs. 3(a)-(c), EDS line analysis across the dark grey region arbitrarily selected from the laser-alloyed surface layer corresponding to case A1 was performed (see Fig. 6(a)). The elemental distribution along the marked line L1 in Fig. 6(a) is illustrated in Fig. 6(b). It is seen that the concentration of Si elements in the dark grey region is significantly higher than that in the light grey region; however, the concentration of Zr element is opposite. At the same time, there is significant elemental diffusion from the dark grey region to the light grey region, indicating the presence of interfacial compounds between these two regions. For further quantitative characterization, the element concentrations in the dark grey region and light grey region, as well as the interface between these two regions, were determined by EDS point analysis (marked as spots 1, 2, and 3). Fig. 7(a) presents the corresponding results. For spot 1, almost only Si and C elements are detected, confirming that the dark grey regions represent the SiC particles. In contrast, spot 2 is mainly composed of C and Zr elements, which suggests that the ZrC phases revealed in the XRD patterns of Fig. 5 may mainly exist in the interfacial region. As for spot 3, it mainly includes the elements contained in the MG substrate (Zr, Ti, Cu and Ni) rather than Si or C elements, indicating that the light grey regions probably represent the MG matrix. To verify the above conjecture, Fig. 7(b) provides the Raman spectral patterns for the above selected three spots. The results indicate that the dark grey region is made of the SiC phase, and the interfacial region is composed of ZrC and SiC phases. Moreover, the absence of any sharp peaks on the Raman spectral pattern for spot 3 confirms that the light grey region retains amorphous characteristics.

Combined with the above XRD, EDS and Raman spectroscopy analysis, it can be concluded that the dark grey region and the light grey region within the laser-alloyed surface layer represent the SiC particles and the MG matrix, respectively. It is well known that phase composition determines the mechanical properties [47], and accordingly, the

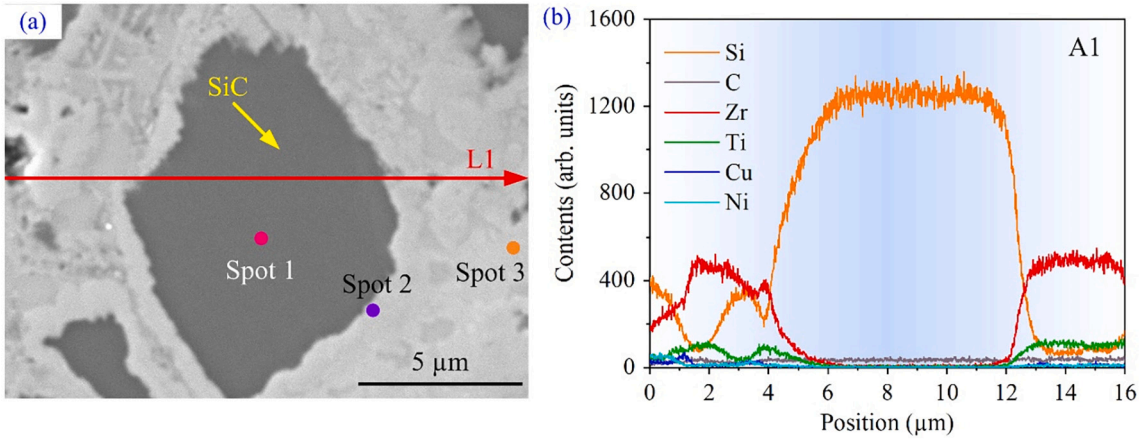

Fig. 6. (a) The position of EDS line analysis and (b) elemental distribution along the marked line L1 in Fig. 6(a).

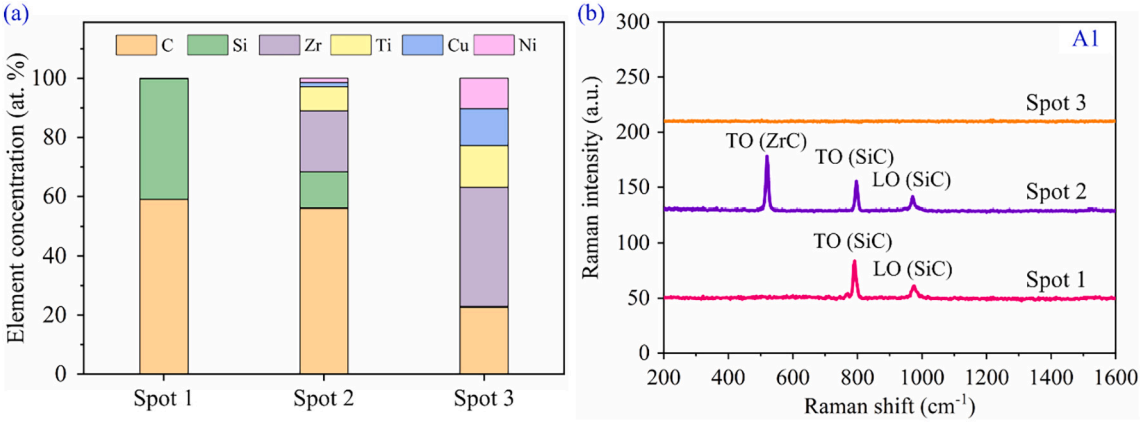

Fig. 7. (a) Elemental concentration and (b) Raman spectrum patterns of the marked spots in Fig. 6(a).

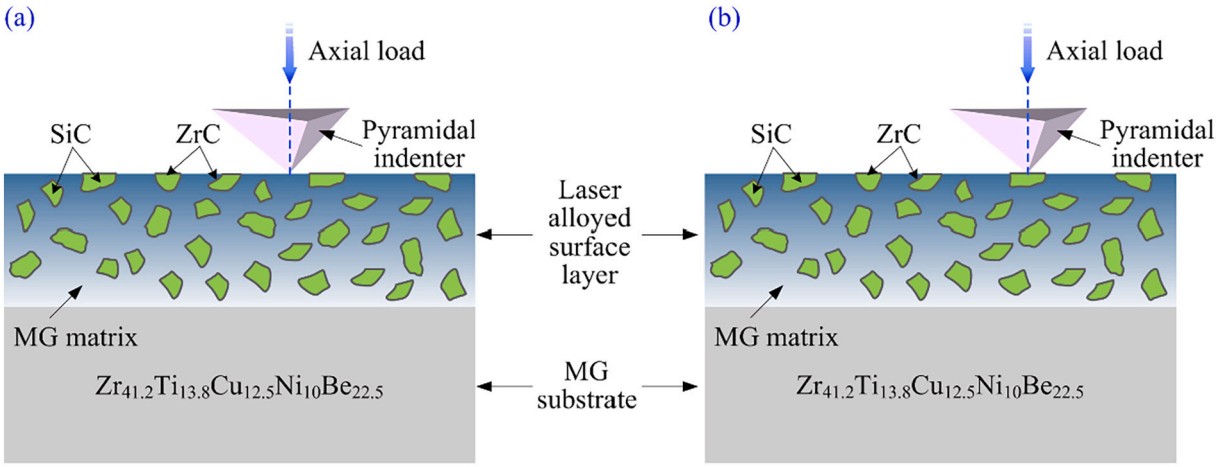

Fig. 8. Schematic diagrams illustrating the indentation positions in nanoindentation measurement: (a) MG matrix and (b) SiC particles.

mechanical properties of SiC particles and MG matrix within the laser-alloyed layers may have large differences. To confirm this, for each tested case, nanoindentation tests were performed on the MG matrix and the SiC particles, respectively, as illustrated in Fig. 8.

Fig. 9(a) presents the hardness of the MG matrix and SiC particles for the three tested cases. For comparison, the hardness of the as-cast specimen is also given in Fig. 9(a). The bars associated with each average hardness value represent the standard deviation of each set of hardness measurements. As shown in Fig. 9(a), the as-cast specimen has an average hardness of 6.46 GPa with a relatively small standard deviation, indicating that its surface mechanical property is considerably homogeneous. For all three tested cases, the SiC particles within the laser-alloyed surface layers exhibit a high hardness being over 30 GPa, which is approximately 4 times higher than that of the as-cast specimen. Surprisingly, the average hardness of the MG matrix within the laser-alloyed surface layers is also significantly higher than that of the as-

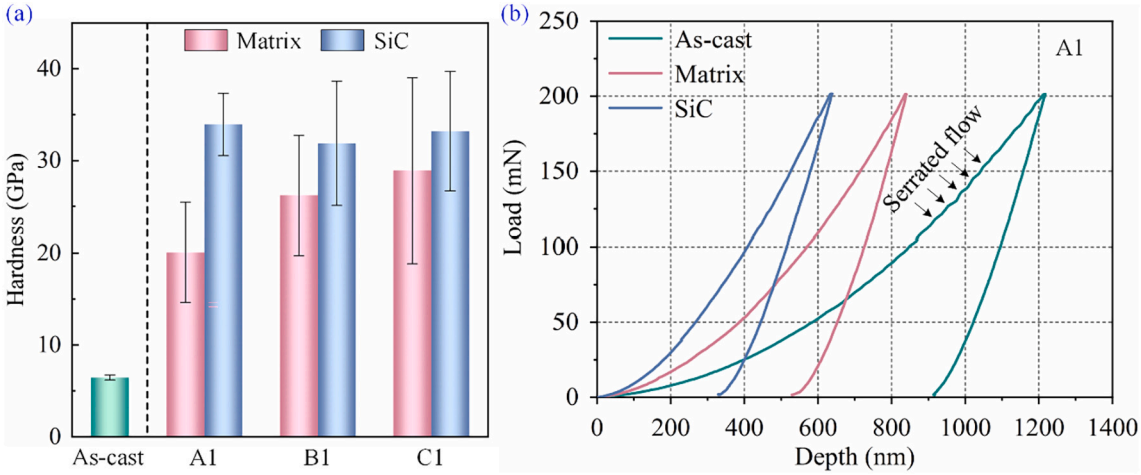

Fig. 9. (a) The hardness of the MG matrix and SiC particle within the laser-alloyed surface layers corresponding to the three tested cases. (b) The representative load-depth curves of the MG matrix and SiC particle within the laser-alloyed surface layer corresponding to case A1. For comparison, the results of the as-cast specimen are also included.

cast specimen. For case A1, the MG matrix within the laser-alloyed surface layer has an average hardness of 20.05 GPa, showing an increase of more than 2 times over that of the as-cast specimen. Furthermore, the average hardness of the MG matrix within the laser-alloyed surface layers corresponding to cases B1 and C1 reaches 26.22 and 28.91 GPa, respectively, which is very close to that of the SiC particles within the laser-alloyed surface layers. This substantial increase in hardness of the MG matrix might be due to the following reason. When nanoindentation experiments are performed on the MG matrix, the SiC particles and in-situ formed ZrC phase around the MG matrix can provide a high resistance to plastic deformation, resulting in enhanced hardness. Moreover, the increase in average hardness of the MG matrix within the laser-alloyed surface layer from case A1 to cases B1 and C1 might be attributed to the increased content of ZrC phase induced by the increased average laser power and overlap ratio during laser surface alloying.

Fig. 10(b) presents representative load-depth curves of the MG matrix and SiC particle within the laser-alloyed surface layer corresponding to case A1. For comparison, the load-depth curve of the as-cast specimen is also included. The maximum penetration depth for the MG matrix and SiC particle is significantly smaller than that for as-cast specimen, which is consistent with the hardness measurement results. In addition, unlike the pronounced serrated flows exhibited by the load-depth curve of the as-cast specimen, a smooth loading curve is observed for the MG matrix, indicating that the microplastic deformation behavior of the fabricated laser-alloyed surface layer is different from that of the as-cast specimen. This can be further confirmed by analyzing the representative residual indent morphologies displayed in Fig. 10. It is seen that macroscopic shear bands appear around the indent of the as-cast specimen, but they almost disappear for the MG matrix. Generally, the pronounced serrated flows on the load-depth curve usually correspond to apparent shear bands near the indents [48,49], and this is consistent with the case in the present study. Furthermore, radial cracks are observed around the residual indent for the SiC particle, which is due to its intrinsic high brittleness [50].

The above analysis of the laser-alloyed surface layers is performed in the horizontal plane; however, from an engineering application point of view, the cross-sectional characteristics of the laser-alloyed surface layers also need to be investigated because they have a significant influence on the service life of the laser-alloyed sample under harsh service conditions. For this purpose, EDS line analysis and hardness measurement were performed on the cross-sections of the laser-alloyed samples corresponding to the three tested cases. These cross-sections were prepared via diamond wire cutting, followed by polishing using diamond abrasive paste. Figs. 11(a), (c) and (e) show the SEM micrographs of the polished cross-sections for cases A1, B1 and C1, respectively, and Figs. 11(b), (d) and (f) present the element distribution along the marked lines in Figs. 11(a), (c) and (e), respectively. The SEM micrographs of the cross-sections for the three tested cases reveal that the SiC particles are uniformly dispersed in the laser-alloyed surface layers (see Figs. 11(a), (c) and (e)). Moreover, for all three cases, the laser-alloyed surface layer and the MG substrate can be easily distinguished on the basis of morphological observation and elemental distribution. As shown in Figs. 11 (b), (d) and (f), the thickness of the laser-alloyed surface layer corresponding to case A1 is 62.29 μm, and it is increased to 68.42 and 71.39 μm for cases B1 and C1, respectively. This is due to

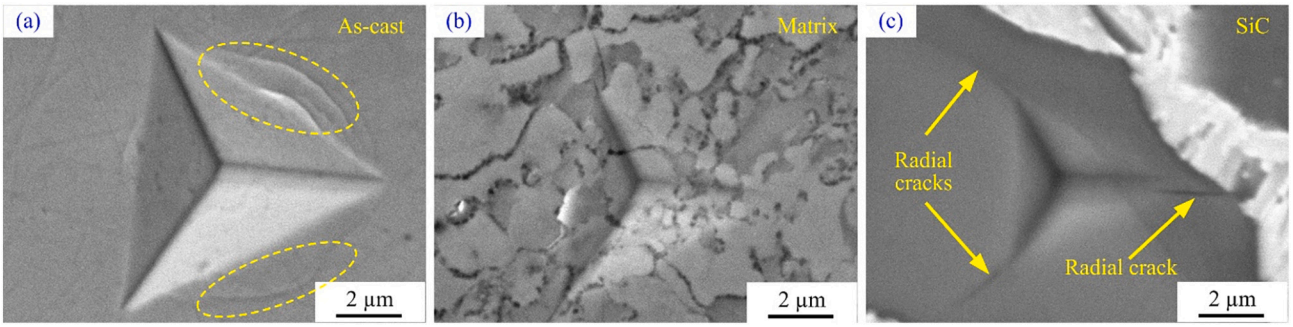

Fig. 10. Representative morphologies of residual indents for (a) as-cast specimen, (b) MG matrix and (C) SiC particle within the laser-alloyed surface layer corresponding to case A1.

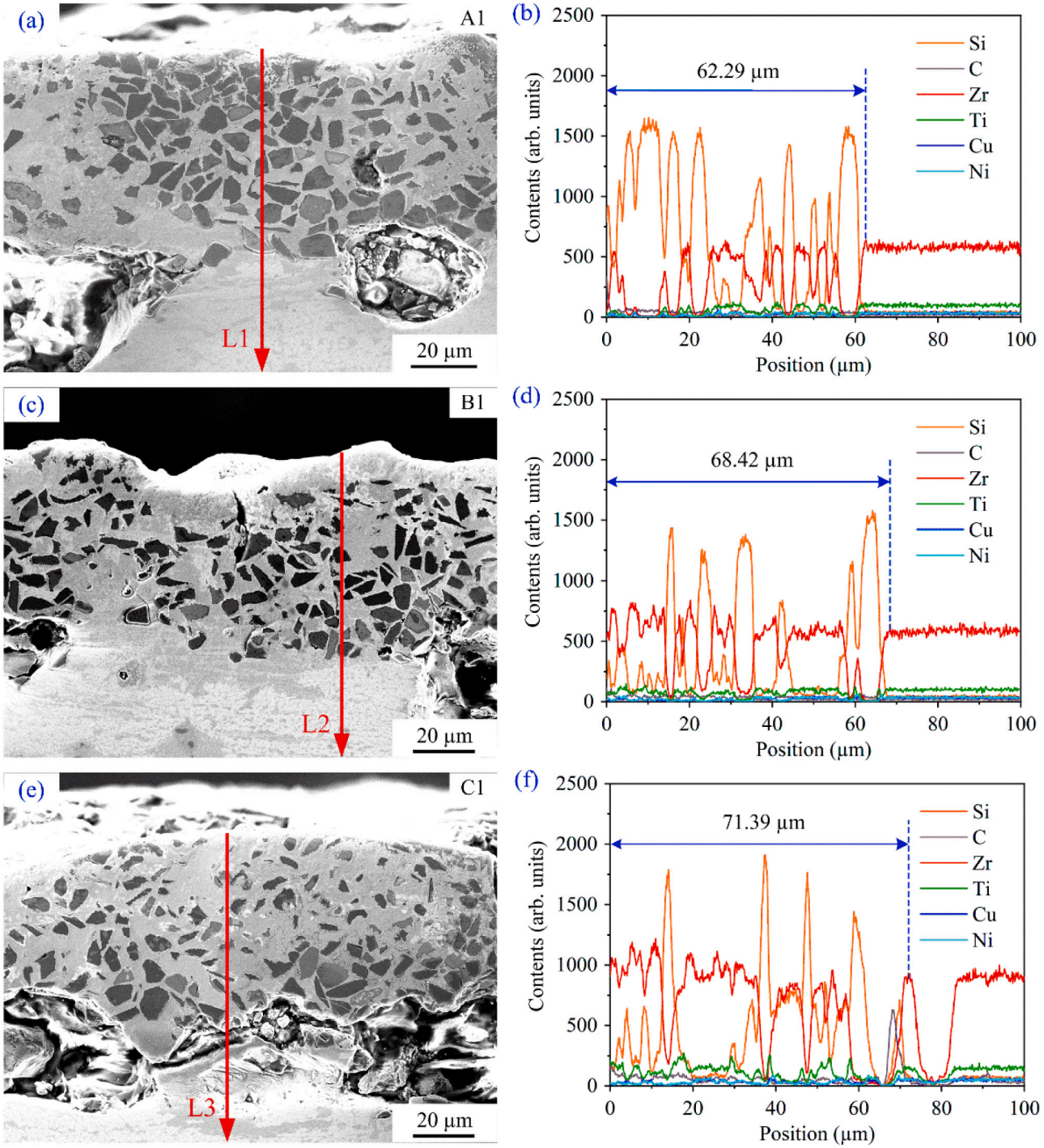

Fig. 11. The SEM micrographs of the cross-sections for the three tested cases: (a) case A1, (c) case B1, and (e) case C1. (b), (d) and (f) present the elemental distribution along the marked lines in Figs. 11(a), (c) and (e), respectively.

that when increasing the average laser power or overlap ratio, more laser energy will be delivered to the MG substrate pre-coated with SiC powder, resulting in a more severe ablation, and correspondingly, a thicker laser-alloyed surface layer will be produced.

Fig. 12 presents the cross-sectional hardness distribution of the laser-alloyed samples corresponding to the three cases investigated. For all three cases, the maximum hardness values occur in the subsurface layer with some distance from the top surface layer, which may be due to its denser microstructure. Moreover, although the average hardness of the laser-alloyed layers corresponding to the three tested cases exhibits obvious difference at different depths, they are all approximately 17–23 GPa higher than the MG substrate. As mentioned above, this substantial increase in hardness could be attributed to the presence of the hard ZrC and SiC ceramic phases within the laser-alloyed surface layers.

4. Conclusions and outlook

In summary, SiC particle reinforced Zr-based MG surface composite layers were successfully fabricated via laser surface alloying. The influences of laser processing parameters, including average laser power and overlap ratio between neighboring laser processing lines, on the microstructure and mechanical properties of the laser-alloyed surface

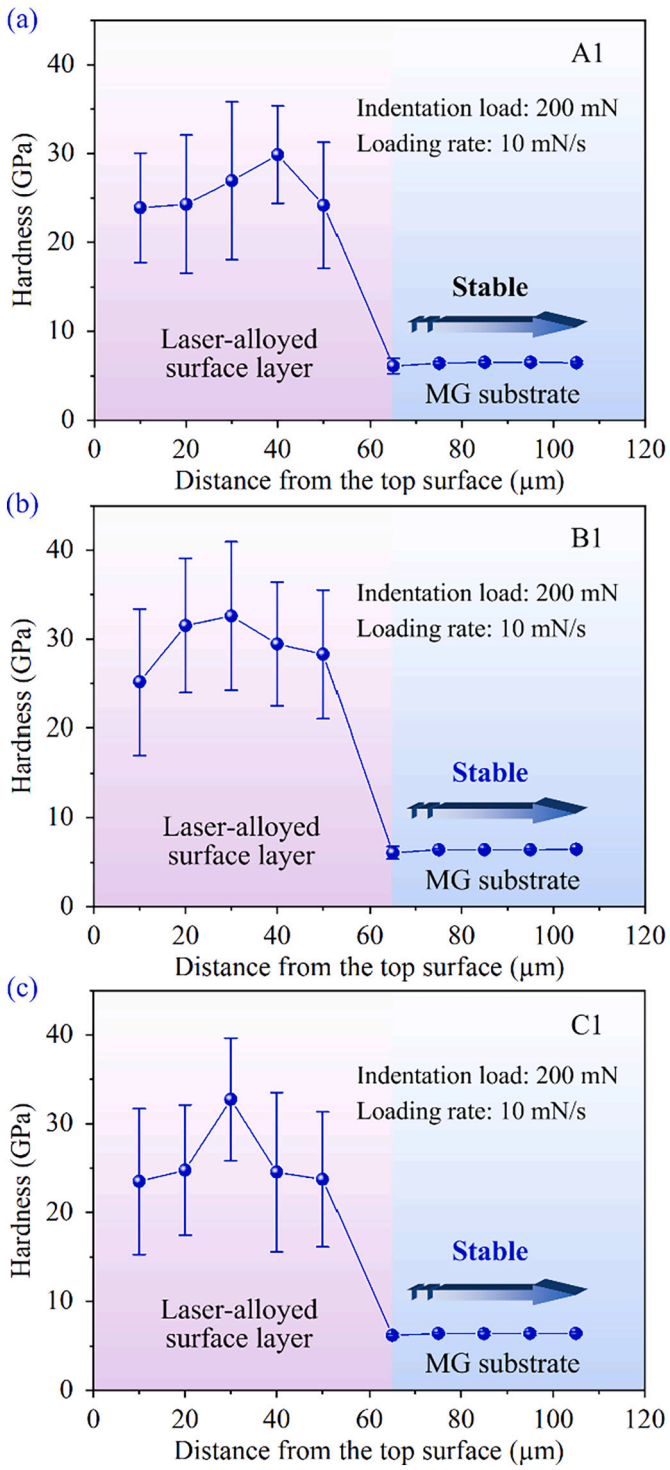

Fig. 12. The cross-sectional hardness distribution of the laser-alloyed samples corresponding to the three cases investigated: (a) case A1, (b) case B1, and (c) case C1.

layer were investigated in detail. Based on the experimental results and analysis, several conclusions could be drawn as follows:

(1) For all cases, SiC particles were uniformly distributed in the laser-alloyed surface layers. The average size of SiC particles within the laser-alloyed surface layer was decreased with the increase of the average laser power or overlap ratio, which could be due to that increasing the input energy would promote the decomposition of SiC particles.

(2) The results of chemical composition analysis indicated that the ZrC and SiC phases were introduced into the MG matrix after laser surface alloying. Among them, the SiC phase rooted in incompletely decomposed SiC particles, and the formation of ZrC phase was due to the in-situ reaction between the Zr atoms root in the MG matrix and the C atoms resulting from the decomposition of the SiC particle.

(3) The generated laser-alloyed surface layers exhibited a significant improvement in overall hardness and changed the microplastic deformation behavior compared with the as-cast specimen. At a relatively high overlap ratio of 70%, the MG matrix within the laser-alloyed surface layer had an average hardness of 28.91 GPa, increasing by over 3 times compared with the as-cast specimen (6.46 GPa). This substantial increase in hardness originated from the presence of the hard ZrC and SiC ceramic phases.

(4) Cross-sectional analysis revealed that the average hardness of the laser-alloyed surface layer at different depths was significantly higher than that of the MG substrate. Moreover, the thickness of the laser-alloyed surface layer was dependent on the employed laser processing parameters.

It should be noted that although the laser-alloyed surface layers with high hardness were successfully fabricated on the MG substrate, some defects such as pores and cracks were observed at the interface between the MG substrate and the laser-alloyed surface layer (see Figs. 11(a), (c) and (e)), which would significantly deteriorate the overall properties of the fabricated laser-alloyed sample. With this in mind, the experimental conditions including the thickness of the pre-coated powder and laser processing parameters will be further optimized in our future work, aiming to obtain defect-free laser-alloyed samples with good mechanical properties.

CRediT authorship contribution statement

Yongfeng Qian: Investigation, Formal analysis, Data curation, Writing - original draft. **Di Zhang:** Investigation, Methodology, Data curation. **Jing Hong:** Investigation. **Lin Zhang:** Data curation. **Minqiang Jiang:** Methodology. **Hu Huang:** Conceptualization, Funding acquisition, Methodology, Resources, Supervision, Writing - review & editing. **Jiwang Yan:** Supervision.

Declaration of competing interest

The authors declare that they have no known competing financial interests or personal relationships that could have appeared to influence the work reported in this paper.

Data availability

Data will be made available on request.

Acknowledgements

This work was supported by the National Natural Science Foundation of China (Grant No. 51705197), the Graduate Innovation Fund of Jilin University (Grant No. 101832020CX106), the Opening Project of the Key Laboratory of CNC Equipment Reliability, Ministry of Education, Jilin University (Grant No. 202104), and the Fundamental Research Funds for the Central Universities (2019-2022).

References

[1] A. Hirata, L.J. Kang, T. Fujita, B. Klumov, K. Matsue, M. Kotani, A.R. Yavari, M. W. Chen, Geometric frustration of icosahedron in metallic glasses, Science 341 (2013) 376–379.

[2] C. Zhang, D. Ouyang, S. Pauly, L. Liu, 3D printing of bulk metallic glasses, Mater. Sci. Eng. R 145 (2021), 100625.

[3] Y.F. Qian, H. Huang, M.Q. Jiang, J.W. Yan, Nanosecond pulsed laser-induced formation of nanopattern on Fe-based metallic glass surface, Appl. Surf. Sci. 577 (2022), 151976.

[4] Y. Wu, D. Cao, Y.L. Yao, G.S. Zhang, J.Y. Wang, L.Q. Liu, F.S. Li, H.Y. Fan, X.J. Liu, H. Wang, X.Z. Wang, H.H. Zhu, S.H. Jiang, P. Kontis, D. Raabe, B. Gault, Z.P. Lu, Substantially enhanced plasticity of bulk metallic glasses by densifying local atomic packing, Nat. Commun. 12 (2021) 6582.

[5] Y.F. Ma, X.F. Tang, X. Wang, M. Zhang, H. Hu, P. Gong, X.Y. Wang, Preparation and mechanical properties of tungsten-particle-reinforced Zr-based bulk-metallic-glass composites, Mater. Sci. Eng. A 815 (2021), 141312.

[6] M.Z. Ibrahim, A.A.D. Sarhan, T.Y. Kuo, F. Yusof, M. Hamdi, T.M. Lee, Developing a new laser cladded FeCrMoCB metallic glass layer on nickel-free stainless-steel as a potential superior wear-resistant coating for joint replacement implants, Surf. Coat. Technol. 392 (2020), 125755.

[7] Y.F. Qian, H. Huang, C. Wang, P. Yu, J.K. Xu, Z.Y. Zhang, Formation of leaf-shaped microstructure on Zr-based metallic glass via nanosecond pulsed laser irradiation, J. Manuf. Process. 72 (2021) 61–70.

[8] S.B. Zhang, P.J. Hou, S. Mooraj, W. Chen, Printability of Zr41.2Ti13.8Cu12.5Ni10.0Be22.5 metallic glass on steel by laser additive manufacturing: a single-track study, Surf. Coat. Technol. 428 (2021), 127882.

[9] A. Malachowska, G. Paczkowski, T. Lampke, A. Ambroziak, Characterization of FeP-based metallic glass coatings prepared with laser cladding, Surf. Coat. Technol. 405 (2021), 126733.

[10] M.X. Li, Y.T. Sun, C. Wang, L.W. Hu, S. Sohn, J. Schroers, W.H. Wang, Y.H. Liu, Data-driven discovery of a universal indicator for metallic glass forming ability, Nat. Mater. 21 (2022) 165–172.

[11] A. Inoue, A. Takeuchi, Recent development and application products of bulk glassy alloys☆, Acta Mater. 59 (2011) 2243–2267.

[12] M. Telford, The case for bulk metallic glass, Mater. Today 7 (2004) 36–43.

[13] A. Inoue, N. Nishiyama, New bulk metallic glasses for applications as magnetic-sensing, chemical, and structural materials, MRS Bull. 32 (2011) 651–658.

[14] S.J. Lorenz, F. Sadeghi, H.K. Trivedi, L. Rosado, M.S. Kirsch, C. Wang, An approach for predicting failure mechanism in rough surface rolling contact fatigue, Tribol. Int. 158 (2021), 106923.

[15] C.H. Li, X.L. Kang, W. Han, W.G. Zheng, L.B. Su, Nanosecond laser-induced surface damage and material failure mechanism of single crystal CaF2 (111) at 355 nm, Appl. Surf. Sci. 480 (2019) 1070–1077.

[16] J. Krell, A. Röttger, U. Ziesing, W. Theisen, Influence of precipitation hardening on the high-temperature sliding wear resistance of an aluminium alloyed iron-nickel base alloy, Tribol. Int. 148 (2020), 106342.

[17] M.A. Hernandez, K.D. Bakoglidis, P. Xiao, A new slurry infiltration method to enhance the wear resistance of bulk graphite with development of reinforced graphitic composites including SiC or Si3N4 hard particles, J. Eur. Ceram. Soc. 39 (2019) 1984–1992.

[18] A.L. Greer, K.L. Rutherford, I.M. Hutchings, Wear resistance of amorphous alloys and related materials, Int. Mater. Rev. 47 (2013) 87–112.

[19] Y.F. Qian, M.Q. Jiang, Z.Y. Zhang, H. Huang, J. Hong, J.W. Yan, Microstructures and mechanical properties of Zr-based metallic glass ablated by nanosecond pulsed laser in various gas atmospheres, J. Alloys Compd. 901 (2022), 163717.

[20] Z.J. Yu, W. Zheng, Z.Q. Li, Y.Z. Lu, X.B. Yun, Z.X. Qin, X. Lu, Accelerated exploration of TRIP metallic glass composite by laser additive manufacturing, J. Mater. Sci. Technol. 78 (2021) 68–73.

[21] J.V. Carstensen, R. Lotfi, W. Chen, S. Szyniszewski, S. Gaitanaros, J. Schroers, J. K. Guest, Topology-optimized bulk metallic glass cellular materials for energy absorption, Scr. Mater. 208 (2022), 114361.

[22] J. Pan, Y.P. Ivanov, W.H. Zhou, Y. Li, A.L. Greer, Strain-hardening and suppression of shear-banding in rejuvenated bulk metallic glass, Nature 578 (2020) 559–562.

[23] L. Zhang, R.L. Narayan, H.M. Fu, U. Ramamurty, W.R. Li, Y.D. Li, H.F. Zhang, Tuning the microstructure and metastability of β-Ti for simultaneous enhancement of strength and ductility of Ti-based bulk metallic glass composites, Acta Mater. 168 (2019) 24–36.

[24] S. Chen, W.Q. Li, L. Zhang, H.M. Fu, Z.K. Li, Z.W. Zhu, H. Li, H.W. Zhang, A. M. Wang, Y.D. Wang, H.F. Zhang, Dynamic compressive mechanical properties of the spiral tungsten wire reinforced Zr-based bulk metallic glass composites, Compos. Part B Eng. 199 (2020), 108219.

[25] H.F. Tian, J.W. Qiao, H.J. Yang, Y.S. Wang, P.K. Liaw, A.D. Lan, The corrosion behavior of in-situ Zr-based metallic glass matrix composites in different corrosive media, Appl. Surf. Sci. 363 (2016) 37–43.

[26] J.W. Qiao, H.L. Jia, P.K. Liaw, Metallic glass matrix composites, Mater. Sci. Eng. R 100 (2016) 1–69.

[27] J.W. Qiao, A.C. Sun, E.W. Huang, Y. Zhang, P.K. Liaw, C.P. Chuang, Tensile deformation micromechanisms for bulk metallic glass matrix composites: from work-hardening to softening, Acta Mater. 59 (2011) 4126–4137.

[28] Y.L. Tang, R.F. Wu, Z.M. Jiao, X.H. Shi, Z.H. Wang, J.W. Qiao, Shear softening of Ta-containing metallic glass matrix composites upon dynamic loading, Mater. Sci. Eng. A 704 (2017) 322–328.

[29] L. Deng, L. Zhang, K. Kosiba, R. Limbach, L. Wondraczek, G. Wang, D.D. Gu, U. Kühn, S. Pauly, CuZr-based bulk metallic glass and glass matrix composites fabricated by selective laser melting, J. Mater. Sci. Technol. 81 (2021) 139–150.

[30] Y. Chen, M.Q. Jiang, L.H. Dai, Collective evolution dynamics of multiple shear bands in bulk metallic glasses, Int. J. Plast. 50 (2013) 18–36.

[31] X.H. Gao, X. Lin, Q.D. Yan, Z.H. Wang, X.B. Yu, Y.H. Zhou, Y.L. Hu, W.D. Huang, Effect of Cu content on microstructure and mechanical properties of in-situ β phases reinforced Ti/Zr-based bulk metallic glass matrix composite by selective laser melting (SLM), J. Mater. Sci. Technol. 67 (2021) 174–185.

[32] Y.M. Shao, W.J. Zheng, W. Guo, S. Lü, S.S. Wu, In-situ Fe-rich particle reinforced Mg-based metallic glass matrix composites via dealloying in metallic melt, Mater. Lett. 285 (2021), 129165.

[33] J. Hong, Y.F. Qian, L. Zhang, H. Huang, M.Q. Jiang, J.W. Yan, Laser nitriding of Zr-based metallic glass: an investigation by orthogonal experiments, Surf. Coat. Technol. 424 (2021), 127657.

[34] Y.X. Li, J.H. Nie, Z.G. Liang, P.K. Bai, Y.X. Yang, B.W. Chen, S.Y. Liu, Q.F. Guan, J. Cai, Microstructure evolution and high-temperature oxidation behavior of FeCrAlNbNi alloyed zone prepared by laser surface alloying on 304 stainless steel, J. Alloys Compd. 888 (2021), 161468.

[35] F. Weng, H.J. Yu, X.Y. Du, H.F. Tian, C.Z. Chen, In-situ formed TiB2/TiC complex structure in laser-alloyed coatings with improved wear property, Ceram. Int. 48 (2022) 7056–7062.

[36] Y.W. Yang, V.A.M. Cristino, L.M. Tam, K.H. Lo, C.T. Kwok, Laser surface alloying of copper with Cr/Ti/CNT for enhancing surface properties, J. Mater. Res. Technol. 17 (2022) 560–573.

[37] Y. Pazhouhanfar, A.S. Namini, S. Shaddel, Z. Ahmadi, M.S. Asl, Combined role of SiC particles and SiC whiskers on the characteristics of spark plasma sintered ZrB2 ceramics, Ceram. Int. 46 (2020) 5773–5778.

[38] Y. Thooyavan, L.A. Kumaraswamidhas, R.E. Raj, J.S. Binoj, Influence of SiC micro and nano particles on tribological, water absorption and mechanical properties of basalt bidirectional mat/vinyl ester composites, Compos. Sci. Technol. 219 (2022), 109210.

[39] T. Wang, Q. Song, S.Y. Zhang, K. Li, C.X. Xiao, H.J. Lin, Q.L. Shen, H.J. Li, Simultaneous enhancement of mechanical and electrical/thermal properties of carbon fiber/polymer composites via SiC nanowires/graphene hybrid nanofillers, Compos.A: Appl. Sci. Manuf. 145 (2021), 106404.

[40] H.G. Huang, H.B. Ke, P. Zhang, Z. Pu, D.L. Zou, P.G. Zhang, T. Shi, L. Zhang, T. W. Liu, U-involved sphere-dispersed metallic glass matrix composites, Mater. Des. 157 (2018) 371–376.

[41] L. Zhang, H.M. Fu, H. Li, Z.W. Zhu, H.W. Zhang, W.R. Li, Y.D. Li, H.F. Zhang, Developing β-type bulk metallic glass composites from Ti/Zr-based bulk metallic glasses by an iteration method, J. Alloys Compd. 740 (2018) 639–646.

[42] C.L. Qiu, N.J.E. Adkins, M.M. Attallah, Microstructure and tensile properties of selectively laser-melted and of HIPed laser-melted Ti–6Al–4V, Mater. Sci. Eng. A 578 (2013) 230–239.

[43] C.L. Qiu, C. Panwisawas, M. Ward, H.C. Basoalto, J.W. Brooks, M.M. Attallah, On the role of melt flow into the surface structure and porosity development during selective laser melting, Acta Mater. 96 (2015) 72–79.

[44] Y. Cao, H.L. Wei, T. Yang, T.T. Liu, W.H. Liao, Printability assessment with porosity and solidification cracking susceptibilities for a high strength aluminum alloy during laser powder bed fusion, Addit. Manuf. 46 (2021), 102103.

[45] H. Huang, Y.F. Qian, C. Wang, J.W. Yan, Laser induced micro-cracking of Zr-based metallic glass using 1011 W/m2 nano-pulses, Mater. Today Commun. 25 (2020), 101554.

[46] B. Adelmann, R. Hellmann, A study of SiC decomposition under laser irradiation, Appl. Phys. A Mater. Sci. Process. 123 (2017) 454.

[47] G. Tosun, M. Kurt, The porosity, microstructure, and hardness of Al-Mg composites reinforced with micro particle SiC/Al2O3 produced using powder metallurgy, Compos. Part B Eng. 174 (2019), 106965.

[48] Y.I. Golovin, V.I. Ivolgin, V.A. Khonik, K. Kitagawa, A.I. Tyurin, Serrated plastic flow during nanoindentation of a bulk metallic glass, Scr. Mater. 45 (2001) 947–952.

[49] H. Huang, M.Q. Jiang, J.W. Yan, The coupling effects of laser thermal shock and surface nitridation on mechanical properties of Zr-based metallic glass, J. Alloys Compd. 770 (2019) 864–874.

[50] X. Yang, X.J. Liu, Z.R. Huang, X.M. Yao, G.L. Liu, Vickers indentation crack analysis of solid-phase-sintered silicon carbide ceramics, Ceram. Int. 39 (2013) 841–845.